THE JOURNAL OF PHYSICAL CHEMISTRY B
A JOURNAL OF THE AMERICAN CHEMICAL SOCIETY

pubs.acs.org/JPCB

Article

Pathways of the Dissociative Electron Attachment Observed in 5- and 6-Azidomethyluracil Nucleosides: Nitrogen (N_2) Elimination vs Azide Anion (N_3^-) Elimination

Daniel Adjei, Yahaira Reyes, Anil Kumar, Samuel Ward, Sergey A. Denisov, Moaadh Alahmadi, Michael D. Sevilla, Stanislaw F. Wnuk,* Mehran Mostafavi,* and Amitava Adhikary*

Cite This: *J. Phys. Chem. B* 2023, 127, 1563−1571

Read Online

ACCESS | Metrics & More | Article Recommendations | Supporting Information

ABSTRACT: 5-Azidomethyl-2′-deoxyuridine (5-AmdU, **1**) has been successfully employed for the metabolic labeling of DNA and fluorescent imaging of live cells. 5-AmdU also demonstrated significant radiosensitization in breast cancer cells via site-specific nitrogen-centered radical (π-aminyl (U-5-CH_2−$NH^\bullet$), **2**, and σ-iminyl (U-5-CH=$N^\bullet$), **3**) formation. This work shows that these nitrogen-centered radicals are not formed via the reduction of the azido group in 6-azidomethyluridine (6-AmU, **4**). Radical assignments were performed using electron spin resonance (ESR) in supercooled solutions, pulse radiolysis in aqueous solutions, and theoretical (DFT) calculations. Radiation-produced electron addition to **4** leads to the facile N_3^- loss, forming a stable neutral C-centered allylic radical (U-6-$CH_2^\bullet$, **5**) through dissociative electron attachment (DEA) via the transient negative ion, TNI (U-6-CH_2-$N_3^{\bullet-}$), in agreement with DFT calculations. In contrast, TNI (U-5-CH_2−$N_3^{\bullet-}$) of **1**, via facile N_2 loss (DEA) and protonation from the surrounding water, forms radical **2**. Subsequently, **2** undergoes rapid H-atom abstraction from **1** and produces the metastable intermediate α-azidoalkyl radical (U-5-$CH^\bullet$-N_3). U-5-$CH^\bullet$-N_3 converts facilely to radical **3**. N_3^- loss from U-6-CH_2−$N_3^{\bullet-}$ is thermodynamically controlled, whereas N_2 loss from U-5-CH_2−$N_3^{\bullet-}$ is dictated by protonation from the surrounding waters and resonance conjugation of the azidomethyl side chain at C5 with the pyrimidine ring.

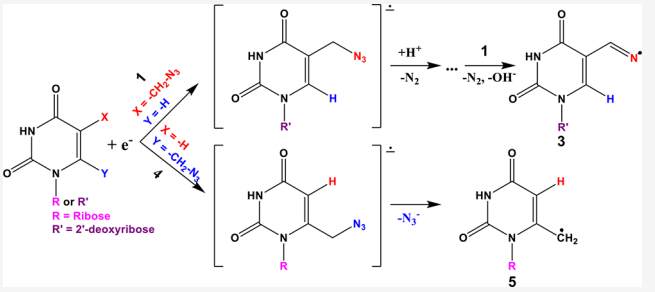

INTRODUCTION

Azido-modified nucleosides have been of interest for over six decades and the finding that 3′-azido-3′-deoxythymidine (AZT or 3′-AZT) is a therapeutic agent[1,2] for acquired immunodeficiency syndrome (AIDS) has sparked interest in their chemistry. The synthesis of azidonucleosides, their reactions, and biological activities have been the subject of several comprehensive reviews.[3,4] Azidonucleosides have been mainly explored as substrates for the (a) synthesis of amino nucleosides, (b) click chemistry, (c) bioconjugation and ligation, (d) enzyme inhibitions including ribonucleotide reductases (RNR),[5,6] among others. Recently, our group is employing azidonucleosides to augment the radiation-induced damage (i.e., radiosensitization) in cancer cells to improve the efficacy of tumor radiotherapy.[7] Apart from our group, a few groups reported substantial radiosensitization provided by 3′-AZT.[8−11] 3′-AZT substantially enhanced γ-irradiation killing of the Epstein−Barr virus (EBV)-transformed lymphoblastoid cells in vitro.[12]

The interaction of ionizing radiation with matter leads to the ejection of high-energy electrons along with ionization and excitation events. These high-energy electrons cause further ionization. These ionization events result in a cascade of medium- and lower-energy electrons that lead to further ionization as well as numerous excited states.[13−18] The DNA radicals (cationic, anionic, and neutral) that are produced through these ionization events and the excited states proximate to these radicals are responsible for most of the subsequent damage to the DNA.[13−16] In addition, low-energy electrons (LEEs) with energies below the ionization threshold can also directly damage the DNA through a dissociative electron attachment process (DEA),[13−26] causing sugar−phosphate bond cleavage, leading to strand break formation.[16,20,21,26]

As the pyrimidines have a stronger electron affinity than purines,[24−32] C5-modified pyrimidine derivatives, for example, C5-halopyrimidine derivatives like 5-bromo-2′-deoxyuridine (5-BrdU) are well-investigated as electron-affinic radiosensi-

Received: November 24, 2022
Revised: January 19, 2023
Published: February 13, 2023

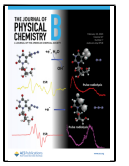

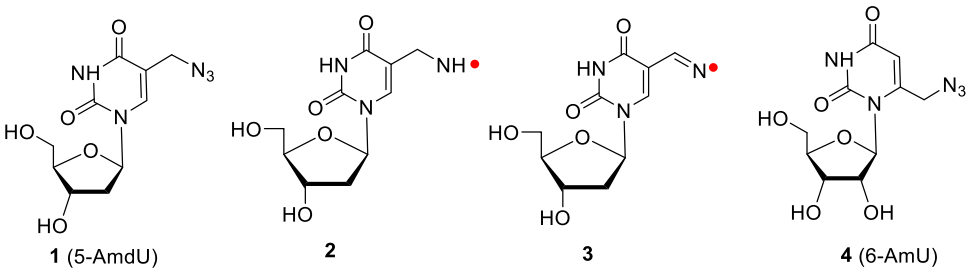

Figure 1. Structures of the compounds and radicals studied in this work. Structures of 5-AmdU (**1**)-mediated π-type aminyl (**2**)/σ-type iminyl radical (**3**). Structure of 6-AmU (**4**).

Scheme 1. Formation of Neutral π-Aminyl Radical, RNH$^\bullet$ (2, U-5-CH$_2$−NH$^\bullet$) from 1, via One-Electron Reduction by Radiation-Produced Electrons[a]

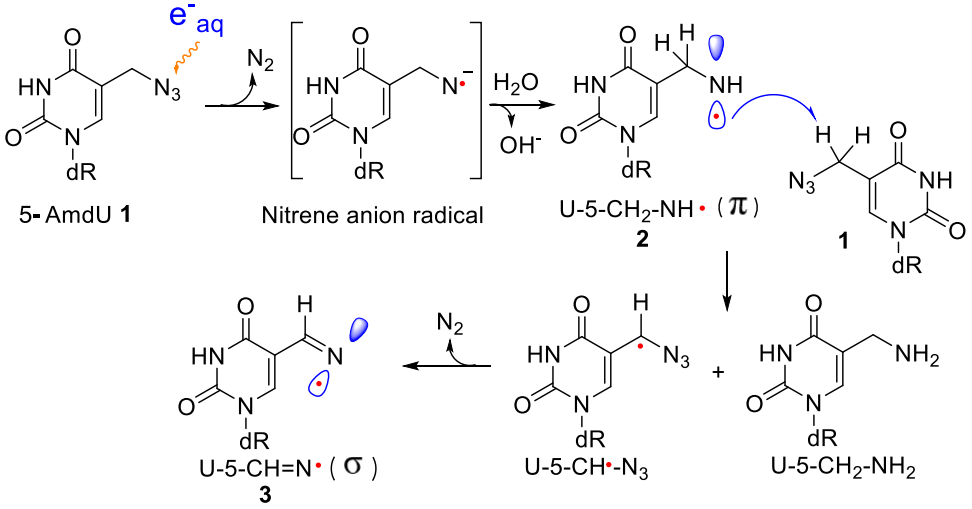

[a]RNH$^\bullet$ from **1** undergoes bimolecular conversion to the σ-minyl radical, R=N$^\bullet$ (**3**, U-5-CH=N$^\bullet$). Reproduced [or adpated, reprinted, etc.] with permission from ref 7, Copyright [2018].

tizers in cancer radiotherapy.[33−40] Cells incorporate 5-BrdU in their DNA almost as readily as thymidine and depending on the extent of 5-BrdU incorporation in cells; as a result, a 3−4-fold increase in radiation-induced cell killing has been reported.[36] However, owing to the toxicity of 5-BrdU, it did not show an increase in patient survival during phase III clinical trials and the trials were called off.[35,37−40] Comparison of the reaction of thymidine (Thd or 5-MedU) and radiation-produced electrons in the gas phase or at low temperatures in the solid state by LEE or a presolvated electron (e_{pre}^-) or at room temperature by a solvated electron (e_{sol}^-), and its previous e_{pre}^-, and by LEE in solution (i.e., quasi-free electrons (e_{qf}^-)) with the corresponding reactions of radiation-produced electrons with 5-BrdU has elucidated the chemical mechanism of radiosensitization provided by 5-BrdU.[35]

We note here that during and after the incorporation of C5-halopyridines in cellular DNA, thymidylate synthetase causes efficient hepatic dehalogenation. This process hinders the accumulation of therapeutically sufficient amounts of halopyrimidines and limits the use of halopyrimidines as effective radiosensitizers for tumor radiotherapy.[35] Therefore, synthesis of C5-halopyridine-like molecules with similar or even better DEA efficiency but without the drawbacks of dehalogenation by thymidylatse synthetase is very crucial. In other words, new base and nucleoside derivatives are synthesized that have similar or better DEA yields in the 0−3 eV region than halopyrimidines,[35] e.g., azidonucleosides. Thus, developing nontoxic and efficient pyrimidine C5-modified analogues as radiosensitizers is of great interest.[29,30,33−35,40]

Neutral π-type aminyl radicals (RNH$^\bullet$) are biologically important and their generation via DEA to azidonucleosides has been investigated by our group through the use of synthesis, electron spin/paramagnetic resonance (ESR/EPR) spectroscopy, and theoretical calculations.[7,24,41−43] These studies have led to the following general findings: (a) base-modified azidopyrimidine nucleosides are found to augment radiation damage to cancerous cells via radiation-produced site-specific electron-mediated π-aminyl (RNH$^\bullet$ (U-5-CH$_2$−NH$^\bullet$), **2**)/σ-iminyl (R=N$^\bullet$ (U-5-CH=N$^\bullet$), **3**) radicals (Figure 1)[7] and (b) the site of azido substitution in the sugar moiety of azidosugars[43] and in the azidopyrimidine nucleoside[42] influences the reactivity (intramolecular vs intermolecular H-atom abstraction) of the aminyl radical. For example, the addition of radiation-produced electrons to 5-azidomethyl-2′-deoxyuridine (5-AmdU, **1** Figure 1) leads to the formation of RNH$^\bullet$, **2**. Radical **2**, via rapid H-atom abstraction from **1**, leads to the formation of the intermediate α-azidoalkyl radical (U-5-CH$^\bullet$-N$_3$). U-5-CH$^\bullet$-N$_3$ undergoes facile N$_2$ loss and conversion to σ-iminyl radical (R=N$^\bullet$), **3** (Scheme 1). 5-AmdU demonstrates effective radiosensitization in EMT6 breast cancer cells.[7]

To expand these studies, 6-azidomethyluridine (6-AmU, **4**, Figure 1) was investigated. Unlike C5-azidomethyl pyrimidine nucleosides,[7] a C6-substituted pyrimidine cannot be incorpo-

https://doi.org/10.1021/acs.jpcb.2c08257
J. Phys. Chem. B 2023, 127, 1563−1571

rated in DNA by a polymerase.[33] We note that **4** is a ribonucleoside and **1** is 2′-deoxyribonucleoside; also, the radicals under investigation are pyrimidine base radicals only and not sugar radicals; the azidomethyl group is bonded to the C6 of the pyrimidine ring in **4** and the azidomethyl group is bonded to the C5 of the pyrimidine ring in **1**. The aims of this work are

(a) to test whether the expected site-specific formation of the same nitrogen-centered (aminyl and iminyl) radicals generated either from the ribonucleoside 6-AmU (**4**) based on our previous studies[7,43] of **1**;

(b) to test whether the initially formed unstable azide anion radical intermediate or the transient negative ion (TNI) (U-6-CH_2-$N_3^{\bullet-}$) leads to the formation of the allylic radical U-6-$CH_2^{\bullet}$, **5**, via unexpected facile loss of azide as an anion (N_3^-) via DEA at 77 K; and

(c) to test whether the same N_3^- loss via DEA happens at room temperature as well. That is, whether temperature could influence the DEA pathway (allylic radical formation due to thermodynamic control at low temperature vs aminyl radical formation via N_2 loss by kinetic control at room temperature).

EXPERIMENTAL SECTION

Synthesis and spectroscopic characterization of **1** including the ESR and theoretical studies of assignments of radicals **2** and **3** along with the EMT6 breast cancer cellular studies showing evidence of radiosensitization by **1** are reported in our previous work.[7] 6-AmU (**4**) was synthesized from uridine employing Tanaka's 6-hydroxymethylation methodolody[44] following the standard mesylation and azidation protocols as described in the Supporting Information.

For ESR studies, methods of preparation of homogeneous glassy samples of **4** and γ-irradiation and storage of these glassy samples including the stepwise annealing of these glassy samples are described in the Supporting Information. The ESR equipment and the experimental setup for recording the ESR spectra at 77 K including field calibration are described in the Supporting Information.

Pulse radiolysis experiments were performed using the ELYSE platform (Paris-Saclay University)[16,20,26,32,35] and the experimental details are provided in the Supporting Information.

Methods of theoretical calculations are described in the Theoretical Calculations section.

RESULTS AND DISCUSSION

ESR Studies. The ESR investigations of 5-azidomethyl-2′-deoxyuridine (5-AmdU, **1** Figure 1) in supercooled (glassy) homogeneous solutions were presented in our previous studies (see Introduction and Scheme 1).[7,43]

To characterize the radical formation via DEA at 77 K from the ribonucleoside (6-AmU, **4**), ESR studies were carried out by employing a γ-irradiated (irradiation at 77 K, absorbed dose = 500 Gy) homogeneous supercooled (glassy, 7.5 M LiBr/D_2O) solution of 6-AmU (**4**). The results of this ESR study are presented in Figure 2.

In Figure 2A, the 77 K ESR spectrum (black) obtained after the addition of radiation-produced prehydrated electrons at 77 K to 6-AmU **4** in a homogeneous oxygen-free aqueous glassy solution at 77 K in the dark (7.5 M LiBr/D_2O) is shown.

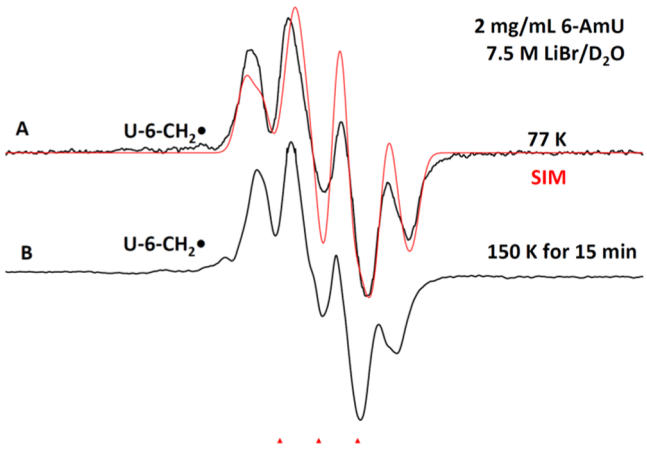

Figure 2. ESR spectrum (black) in (A) after radiation-produced one-electron addition to 6-AmU **4** (2.0 mg/mL) at 77 K (γ-irradiation, 500 Gy) in 7.5 M LiBr/D_2O in dark. Spectrum (black) in (B) was obtained via warming the sample for 15 min at ca. 150 K in the dark. All spectra were recorded at 77 K. The red spectrum in (A) is the simulated spectrum (for simulation parameters, see text). The three reference markers in this figure and in subsequent figures are Fremy's salt resonances with a central marker at g = 2.0056 and each of the three markers is separated from one another by 13.09 G.

We have compared the black spectrum in Figure 2A with our reported spectra[7,41−43] of the π-aminyl radical observed from azidonucleosides and azidosugars at 77 K in the dark. This comparison establishes that spectrum 2A does not show the line components due to axially symmetric anisotropic N-atom at the wings. Rather, the g-values (g_{xx}, g_{yy}, g_{zz} = (2.0030, 2.0030, 2.0023)) demonstrate that this spectrum is due to a C-centered radical. Taking these g-values into account, applying a mixed (Lorentzian/Gaussian = 1) lineshape, an isotropic linewidth of 5.5 G, and using three α-H hyperfine coupling constant values, HFCCs, (A_{xx} = −17.52, A_{xy} = −7.02, A_{yy} = −12.06, A_{zz} = −14.63; A_{xx} = −7.78, A_{xy} =−2.62, A_{yy} =−24.33, A_{zz} = −16.54; A_{xx} = −4.61, A_{yy} = −14.02, A_{zz} = −10.51), a simulated spectrum (red) is obtained. The superimposition of the experimentally recorded (black) with the simulated spectrum (red) in Figure 2A shows a nice match. Based on these results, we have assigned these spectra to the allylic U-6-$CH_2^{\bullet}$, **5**. This radical is a C-centered radical and shows three α-H HFCCs: two at C6 and one at C5.

The spectrum (black) in Figure 2B is obtained after warming the sample at ca. 150 K in the dark for 15 min. This spectrum is only slightly changed from the experimental and simulated spectra shown in Figure 2A. The g-value at the center of spectrum 2B matches that of both experimental (black) and simulated (red) spectra in Figure 2A. Therefore, we have assigned the spectrum 2B to the allylic U-6-$CH_2^{\bullet}$, **5**, as well.

Thus, the ESR studies establish that contrary to our results with **1** where radiation-mediated e_{pre}^-, formed in homogeneous aqueous glassy solution (7.5 M LiCl, 77 K) in the absence of oxygen, leads to the radical **2** that converts to **3** (Scheme 1), radiation-produced e_{pre}^- addition to **4** leads to the unexpected loss of azide as an anion via DEA, from the initially formed TNI (U-6-CH_2−$N_3^{\bullet-}$), to generate the allylic radical **5** (Figure 3).

Pulse Radiolysis. Time-resolved radiolysis of aqueous solutions of **1** and **4** was conducted at room temperature at different concentrations (0.2, 0.5, and 1 mM) in the spectral

https://doi.org/10.1021/acs.jpcb.2c08257
J. Phys. Chem. B 2023, 127, 1563−1571

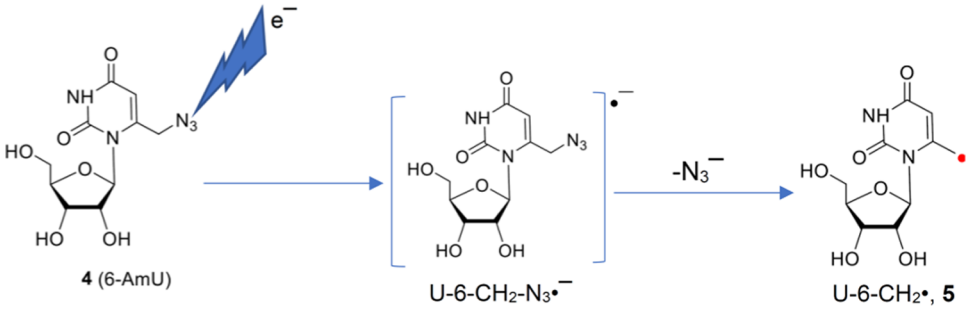

Figure 3. Allylic radical U-6-$CH_2^{\bullet}$, **5**, formation via unexpected loss of azide as an anion (N_3^-) from the azide anion radical intermediate (U-6-CH_2–$N_3^{\bullet-}$) or TNI of **5** via dissociative electron attachment.

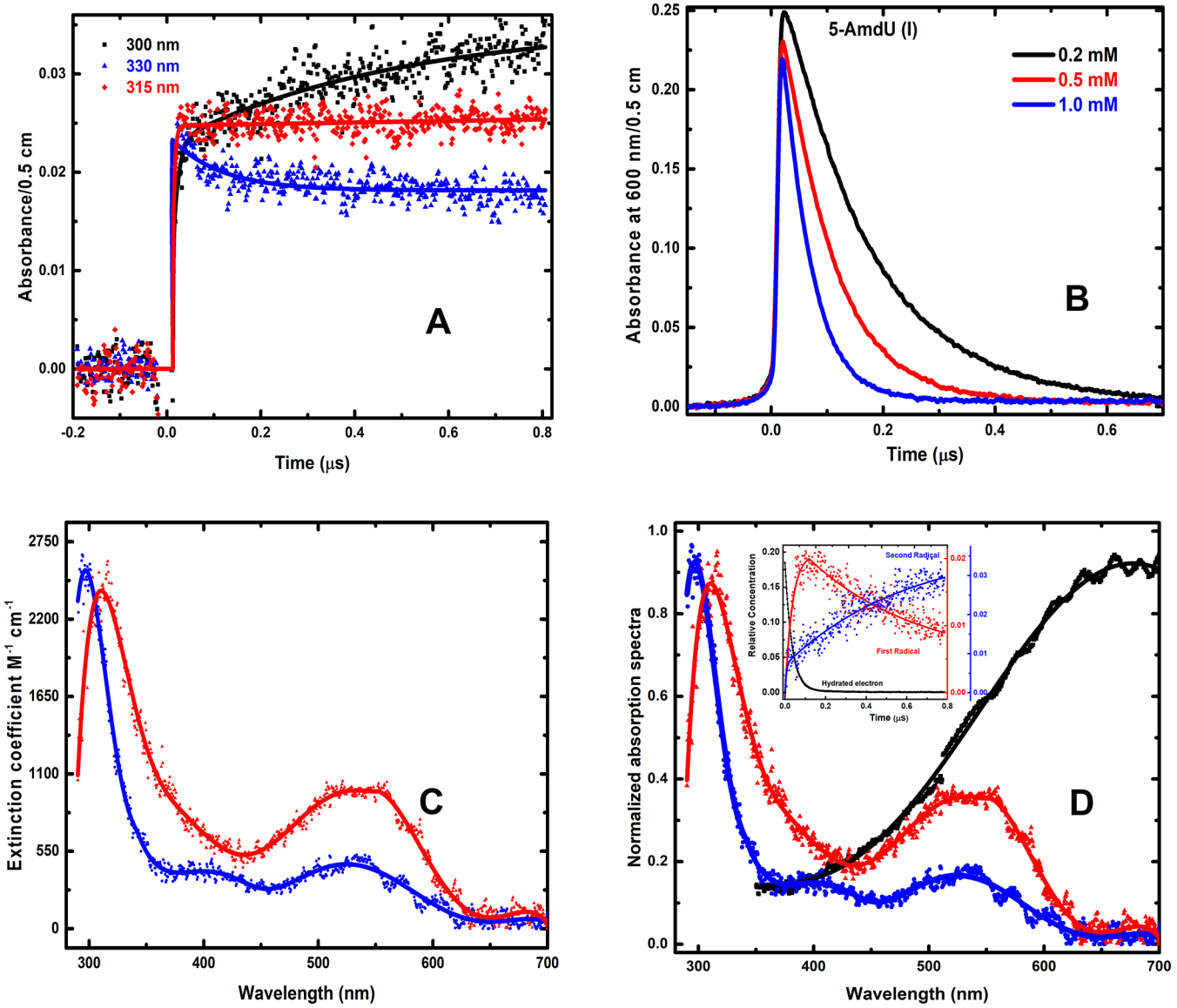

Figure 4. Pulse radiolysis of Ar-saturated solutions of **1** in the presence of 0.2 M *t*-butanol. (A) Kinetics of species formed were observed at 300, 315, and 330 nm for the same solution ([**1**] = 1 mM). (B) The kinetics of electron reaction were observed at 600 nm for three different concentrations (0.2, 0.5, and 1 mM) of **1**. (C) Absolute absorption spectra of the radicals obtained via e_{aq}^- -mediated reduction of **1**. (D) The deconvoluted kinetics of e_{aq}^- and the radicals of **1** ([**1**] = 1 mM) (see inset) and the absorption spectra obtained by Bayesian analysis of full spectro-kinetics data matrix (Figure S1).

range 280–700 nm at different timescales. The solutions were saturated using Ar and contained 0.2 M *t*-butanol to scavenge the hydrogen atom ($H^{\bullet}$) and hydroxyl radical ($^{\bullet}OH$) produced due to water radiolysis.[16,26,29,30,32,45] Therefore, under these conditions, only the hydrated electron, e_{aq}^-, reacts with the solute (**1** or **4**).

https://doi.org/10.1021/acs.jpcb.2c08257
J. Phys. Chem. B 2023, 127, 1563–1571

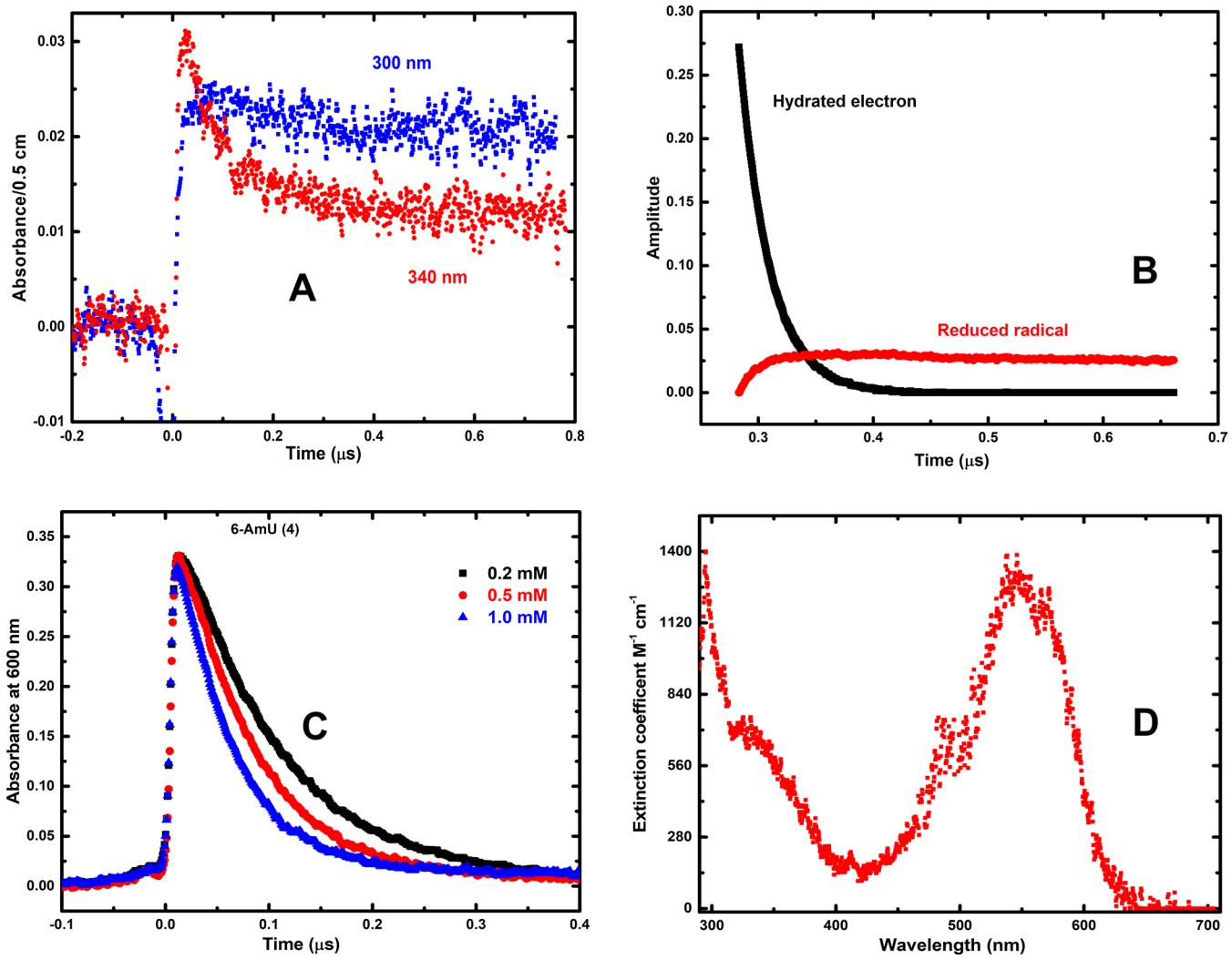

Figure 5. Pulse radiolysis of Ar-saturated solution of **4** in the presence of 0.2 M *t*-butanol. Kinetics of species formed were observed at 300 and 340 nm for the same solution ([**4**] = 1 mM, A). The kinetics were observed at 600 nm for three different concentrations (0.2, 0.5, and 1 mM) of **4** (C). The deconvoluted kinetics of hydrated electron (e^-_{aq}) and the radicals of **4** ([**4**] = 1 mM) (B) and the absorption spectra obtained by Bayesian analysis of full spectro-kinetics data matrix are shown ((D), see also Figure S4). The absolute absorption spectrum of the radical species (**5**) was obtained via the reduction of **4** using an isosbestic point.

Pulse Radiolysis of ***1****.* The increase in the decay of e^-_{aq} absorption at 600 nm correlates with the concentration of **1** (Figure 4B). The rate constant of the reaction between e^-_{aq} and **1** is found to be $(1 \pm 0.2) \times 10^{10}$ M^{-1} s^{-1}; hence, this reaction is diffusion-controlled. The kinetics are wavelength dependent in the UV region (Figure 4), i.e., there could be multiple species involved with different absorption and kinetic properties (vide infra). To illustrate, we reported decay at three selected wavelengths: 300, 315, and 330 nm (Figure 4A).

The data presented in Figure 4 established that along with the decay of e^-_{aq}, an absorption band around 300 nm is formed with a weaker band around 530 nm (Figure 4C,D). Combining our published ESR results on **1**[7,43] and the DFT-calculated UV−vis spectral results (vide infra), we assigned this absorption to **2**. This is further supported by the kinetics in the first 200 ns when e^-_{aq} decays and **2** is formed and reaches a maximum (see inset, Figure 4D). The kinetics measured in the UV region showed that there is an isosbestic point at 315 nm (Figure 4C,D) between the absorption of e^-_{aq} and the species formed successively after the decay of e^-_{aq} (inset, Figure 4D). Therefore, we can deduce that the extinction coefficient of the absorption band of $RNH^\bullet$ at 315 nm is ca. 1180 M^{-1} cm^{-1}.

At 300 nm within 200 ns, we observed only an increase in absorbance (Figure 4A). After the completion of the decay of e^-_{aq}, the global data analysis showed the presence of two transient species: **2** (maximum of absorbance 310 nm with a shoulder around 410 nm) and an absorption band around 540 nm (Figures 4C,D and S1). The band at 540 nm is observed to be ca. 2 times less intense than that at 310 nm. The rate of formation of the final species depends on the concentration of **1**, confirming the bimolecular reaction of radical **2** with **1** to form the α-azidoalkyl radical (U-5-$CH^\bullet$-N_3), supporting our ESR investigations on **1**[7,43] and Scheme 1. From these data, by exploiting the isosbestic point and combining our published ESR results on **1**[7,43] and the DFT-calculated UV−vis spectral results (vide infra and Figures S6−S9), we assigned this absorption to the combination of the α-azidoalkyl radical (U-5-$CH^\bullet$-N_3) and the σ-type iminyl radical, U-C5-CH=$N^\bullet$, **3** (Scheme 1).

Pulse radiolysis of Ar-saturated solutions of **1** ([**1**] = 1 mM) in the presence 0.2 M *t*-butanol at pH = 12 yielded results

https://doi.org/10.1021/acs.jpcb.2c08257
J. Phys. Chem. B 2023, 127, 1563−1571

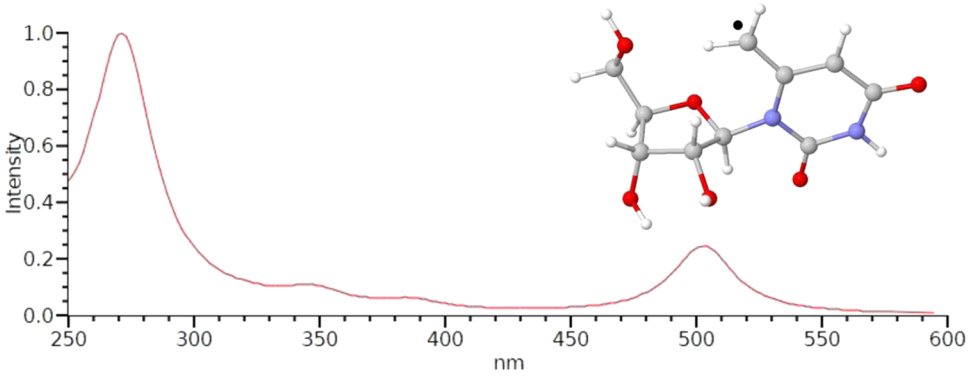

Figure 6. B3LYP-PCM/6-31G++** calculated vertical excited state spectrum of the allylic radical, **5**, from **4**.

(Figures S2 and S3) similar to those presented in Figure 4. These results demonstrate that the formation of radical **2**, α-azidoalkyl radical (U-5-CH$^{\bullet}$-N_3), and σ-type iminyl radical, U-C5-CH=N$^{\bullet}$, **3**, from **1** are not pH dependent. These results agree with our earlier ESR studies showing the RNH$^{\bullet}$ formation from AZT at pH of ca. 5 and 12.[41] Furthermore, these results demonstrate that the protonation from the water molecules surrounding the TNI (U-5-CH_2-$N_3^{\bullet-}$) plays an important role in the N_2 loss that is involved DEA pathway. This is supported by the theoretical calculations (vide infra).

Pulse Radiolysis of 4. Employing solutions of **4** with different concentrations (0.2, 0.5, and 1 mM), we investigated the kinetics between 280 and 700 nm at room temperature (Figure 5).

Similar to pulse radiolysis of **1**, the decay of e_{aq}^- is accelerated in the presence of **4** (Figures 5B and S4). From the decay kinetics at 600 nm (Figure 5C), the rate constant of the reaction between e_{aq}^- and **4** is found to be $(5.5 \pm 0.2) \times 10^9$ M^{-1} s^{-1}, and this reaction is almost diffusion-controlled similar to the corresponding reaction observed in **1**. Although this reaction is slower than the corresponding reaction of e_{aq}^- with **1** by a factor of ca. 2, e_{aq}^- reacts quantitatively with either **1** or **4** due to the diffusion-controlled nature of this reaction.

The decay of e_{aq}^- is correlated with the formation of a species with an absorption spectrum showing a band at 295 nm, a shoulder around 340 nm, and another absorption band located at 550 nm (Figure 5D). In addition, the data analyses of all spectro-kinetics data showed the presence of only two species: e_{aq}^- and the species that resulted due to the reduction of **4** by e_{aq}^- (Figures S4 and 5B). The transient absorption data display a weak isosbestic point, thereby showing that the value of the extinction coefficient of e_{aq}^- and the extinction coefficient of the anion radical (U-6-CH_2-$N_3^{\bullet-}$) is almost the same (Figure 5A, kinetics at 300 nm). Thus, the extinction coefficient of the absorption spectra of radical (Figure 5D) formed via reduction of **4** by e_{aq}^- is deduced. This radical is stable at least for 1 μs.

A comparison of Figures 4 and 5 shows that there are two major differences in the e_{aq}^- reduction of **1** and **4**. The reduction of **1** forms first a very short transient species with a half-lifetime of less than 100 ns. This transient species resulted in an absorption spectrum with bands at 310, a shoulder at 340 nm, and a weak band at 540 nm (Figure 4C,D). This absorption spectrum is assigned to the combination of the α-azidoalkyl radical (U-5-CH$^{\bullet}$-N_3) and σ-type iminyl radical, U-C5-CH=N$^{\bullet}$, **3**.

However, the reduction of **4** by e_{aq}^- forms directly the radical representing an absorption spectrum with a band at 295 nm, a shoulder at 340 nm, and another band at 550 nm (Figure 5D). This band at 550 nm is 2 times more intense than that observed by the reduction of **1** (Figure S5). Based on the ESR results (Figure 2) and DFT calculations (see below), this radical species from **4** is assigned to the allylic radical **5** (Figure 3).

Theoretical Calculations. To support the assignments of the radicals using ESR investigations of homogeneous glassy solutions and pulse radiolysis in dilute aqueous solutions at ambient temperature, theoretical calculations were performed. Density functional theory (DFT) using the B3LYP functional and the 6-31G++** basis set was employed for the structural optimization of radicals in their ground state. Time-dependent density functional theory (TD-DFT) at the same level of theory was applied to calculate the vertical excited states and UV−vis spectra of the C-centered allylic radicals, viz, U-C5-$CH_2^{\bullet}$ (from **1**) and **5** (from **4**), as well the radicals with heteroatoms formed from the ribonucleoside of **1**, viz, the aminyl radical (**2**), the α-azidoalkyl radical (U-5-CH$^{\bullet}$-N_3), and the iminyl radical (**3**). All of the calculations were performed in the aqueous phase employing the integral equation formalism of the polarized continuum model (IEF-PCM) by Tomasi et al.[46] Gaussian 16 suite of programs[47] is used for the calculations. Jmol,[48] a free molecular viewer, is used for drawing the structure, and the spectra were plotted using the Gabedit freeware.[49]

HFCC Calculation of the Allylic Radical (5). The B3LYP-PCM/6-31G++** calculated isotropic HFCCs (A_{iso}) of three hydrogens (the two hydrogens of the CH_2 group attached at C6 and H5 attached at C5) of **5** from **4** are H5 (−11.4 G), H6′ (−16.2 G), and H6″ (−15.3 G). The calculated anisotropic HFCCs (A_{aniso}) of these hydrogens are H5 [−5.0, −1.0, 6.0] G, H6′ [−8.8, −0.3, 9.1] G, and H6″ [−7.8, −0.7, 8.5] G, respectively. The total HFCCs (A_{iso} + A_{aniso}) are H5 [−16.4, −12.4, −5.4] G, H6′ [−25, −16.5, −7.1] G, and H6″ [−23.1, −16, −6.8] G, respectively. The corresponding experimental HFCCs are (A_{xx} = −4.61, A_{yy} = −14.02, A_{zz} = −10.51; A_{xx} = −17.52, A_{yy} = −12.06, A_{zz} = −14.63; A_{xx} = −7.78, A_{yy} = −24.33, Azz = −16.54); both sets of HFCCs compare fairly.

Calculated UV−vis Spectra. The B3LYP-PCM/6-31G++** calculated vertical excited state spectrum of **5** presented in Figure 6 shows absorbance peaks at ca. 272, 348, 390, and 503 nm. The peak at ca. 272 nm has the maximum absorbance. The spectrum obtained employing pulse radiolysis of **4** (Figure 5) has maxima absorbance at 295, 340, and 540 nm. The calculated spectrum is blue-shifted by ca. 20 nm, and the

https://doi.org/10.1021/acs.jpcb.2c08257
J. Phys. Chem. B 2023, 127, 1563−1571

Scheme 2. Summary of the Results Establishing that the Position of the Azidomethyl Group or the Azido Group in the Compound and the Surrounding Water Molecules Dictate the Elimination Part (N_2 or N_3^- Loss) of DEA Reaction from the TNI

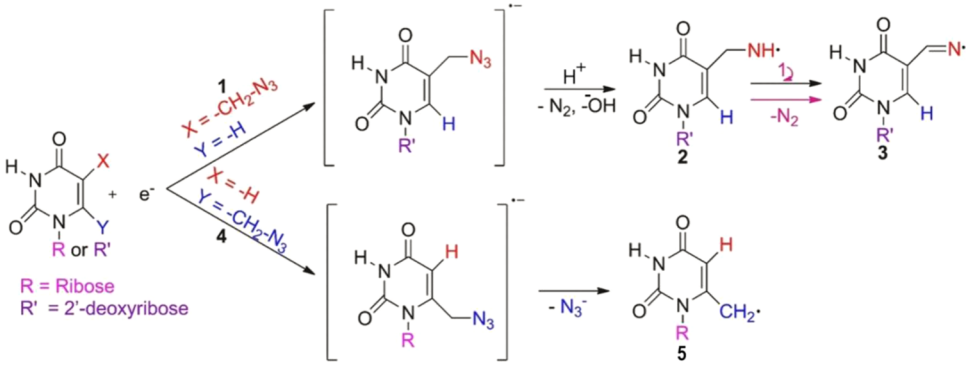

calculated spectrum after a 20 nm shift has peaks at 292, 368, 410, and 523 nm, respectively, which is in good agreement with the experiment. A small discrepancy between theory and experiment is expected,[50] as the present calculations do not consider vibronic and thermal effects.

The spectra of the aminyl radical (**2**), α-azidoalkyl radical (U-5-$CH^{\bullet}$-N_3), and σ-type iminyl radical, R-CH=$N^{\bullet}$ (**3**) are shown in the Supporting Information (Figures S6–S8).

We have also calculated the theoretical excited state spectrum of the allylic U-5-$CH_2^{\bullet}$ from 5-AmU anion radical via azide anion loss (Figure S9). This spectrum does not match with those shown in Figures 5 and 6.

In addition, theoretical calculations show that the TNI of **4** undergoes a barrier-free N_3^- loss. On the other hand, in the B3LYP-PCM/6-31G++** calculated and optimized structure of **1** using the same method, we find that in the azidomethyl moiety at C5, the N1–N2 bond starts at 1.23 A. In the TNI (U-5-CH_2–$N_3^{\bullet -}$) of **1**, i.e., upon adding one electron to **1**, this bond distance becomes 1.33 A and following this, there is a 12 kcal/mol barrier to cause the cleavage of the N1–N2 bond, leading to N_2 loss. From our earlier ESR work on AZT at different pH (ca. 5 and 12)[41] and pulse radiolysis of **1** at different pH (7 and 11, this work), it is possible that the protonation of the TNI (U-5-CH_2–$N_3^{\bullet -}$) of **1** is likely to complete the N1–N2 bond cleavage process required for the N_2 loss. To check this possibility, we calculated (at B3LYP/6-31G**) the barrier for N_2 loss after the protonation of the N1 nitrogen of U-5-CH_2–$N_3^{\bullet -}$ by the water (solvent) molecules and found a nominal barrier of 1.6 kcal/mol (Figure S10). This small barrier confirms that the protonation of U-5-CH_2-$N_3^{\bullet -}$ by the surrounding water molecules will drive the N_2 loss reaction to completion.

CONCLUSIONS

ESR studies in the homogeneous glassy solution, pulse radiolysis in aqueous solution at ambient temperature, and DFT (for HFCCs) along with TD-DFT (for UV–vis spectra) calculations were performed to characterize the radical formed via DEA from **4**. These studies led to an unequivocal identification of highly stable allylic radical **5** (Figure 3). Formation of **5** at 77 K and at the ambient temperature establishes that N_3^- elimination from the TNI of **4** is thermodynamically and not kinetically controlled. Resonance stabilization of **5** owing to the presence of the azidomethyl moiety at position C6 of the base and solvation of N_3^- by the surrounding water molecules contribute to the facile N_3^- loss from the TNI of **4**.

Compound **4** enabled us to compare the radiation chemical results (ESR, pulse radiolysis, and theory) with the already published results[7,43] (ESR and theory) for **1**. The ESR experiments were carried out using a glassy solution, whereas pulse radiolysis experiments were conducted in aqueous solutions at ambient temperatures. ESR and pulse radiolysis results show that the mechanisms are the same in the glassy and aqueous samples and this comparison established that (a) the radicals formed from these two compounds **1** (radicals **2** and **3**, Scheme 1) and **4** (radical **5**, Figure 3) via the same reaction (DEA) are different, and (b) the reaction mechanism of DEA along with the subsequent reactions of the radicals formed are also different (N_2 loss and protonation from the surrounding water (Scheme 1) vs N_3^- loss (Figure 3)).

Pulse radiolysis at various pH and TD-DFT calculations (this work) along with our previous ESR and DFT studies[7,43] establish that the TNI of **1** forms the aminyl radical (**2**, U-C5–$CH_2NH^{\bullet}$) via N_2 loss followed by rapid solvent protonation of the incipient nitrene anion radical. For the N_2 loss, the resultant nitrene anion radical (U-C5-$CH_2N^{\bullet -}$) and the subsequent aminyl radical (**2**) have hyperconjugation stabilization due to two methylene protons. This resonance stabilization and protonation from the surrounding solvent (water molecules) explain our previous observation of aminyl radical formation in the azidonucleosides where the azido group is in the sugar moiety and in aliphatic 3-azido-1-propanol via DEA through N_2 loss. In addition, both ESR[7,43] and pulse radiolysis support the formation of the α-azidoalkyl radical (U-5-$CH^{\bullet}$-N_3) from **1** and its conversion to the σ-type iminyl radical, **3** (Scheme 1).

In conclusion, our work combining synthesis, ESR, pulse radiolysis, and theory establishes that the position of the azidomethyl group or the azido group in the compound and the surrounding water molecules dictate the elimination part (N_2 or N_3^- loss) of DEA reaction from the TNI. N_2 loss from the TNI is the dominant mechanism of the DEA observed in the azido-substituted compounds that we have investigated, so far. TNI of **4** is the only case to date in which we have observed N_3^- loss, leading to the formation of the resonance conjugation stabilized allylic radical **5**. Combining Scheme 1 and Figure 3, the findings of our work are summarized in Scheme 2.

https://doi.org/10.1021/acs.jpcb.2c08257
J. Phys. Chem. B 2023, 127, 1563–1571

■ ASSOCIATED CONTENT

Supporting Information

The Supporting Information is available free of charge at https://pubs.acs.org/doi/10.1021/acs.jpcb.2c08257.

Relevant information for the synthesis of compound **4**, sample preparation and methodologies for ESR studies, methodology and additional data of pulse radiolysis, additional data of theoretical including TD-DFT calculations (PDF)

■ AUTHOR INFORMATION

Corresponding Authors

Stanislaw F. Wnuk − *Department of Chemistry and Biochemistry, Florida International University, Miami, Florida 33199, United States;* orcid.org/0000-0002-3111-3919; Email: wnuk@fiu.edu

Mehran Mostafavi − *Institut de Chimie Physique, UMR 8000 CNRS, Bât. 349, Université Paris-Saclay, 91405 Orsay Cedex, France;* orcid.org/0000-0002-4510-8272; Email: mehran.mostafavi@universite-paris-saclay.fr

Amitava Adhikary − *Department of Chemistry, Oakland University, Rochester, Michigan 48309, United States;* orcid.org/0000-0001-9024-9579; Email: adhikary@oakland.edu

Authors

Daniel Adjei − *Institut de Chimie Physique, UMR 8000 CNRS, Bât. 349, Université Paris-Saclay, 91405 Orsay Cedex, France*

Yahaira Reyes − *Department of Chemistry and Biochemistry, Florida International University, Miami, Florida 33199, United States*

Anil Kumar − *Department of Chemistry, Oakland University, Rochester, Michigan 48309, United States;* orcid.org/0000-0002-9979-7798

Samuel Ward − *Department of Chemistry, Oakland University, Rochester, Michigan 48309, United States*

Sergey A. Denisov − *Institut de Chimie Physique, UMR 8000 CNRS, Bât. 349, Université Paris-Saclay, 91405 Orsay Cedex, France*

Moaadh Alahmadi − *Department of Chemistry, Oakland University, Rochester, Michigan 48309, United States*

Michael D. Sevilla − *Department of Chemistry, Oakland University, Rochester, Michigan 48309, United States;* orcid.org/0000-0001-8799-5458

Complete contact information is available at: https://pubs.acs.org/10.1021/acs.jpcb.2c08257

Notes

The authors declare no competing financial interest.

■ ACKNOWLEDGMENTS

S.W., A.K., M.D.S., and A.A. thank the National Cancer Institute of the National Institutes of Health (Grant RO1CA045424) for support. A.A. thanks the National Science Foundation under Grant No. CHE-1920110. A.A. also thanks Université Paris-Saclay for the Visiting Professorship at the Institut de Chimie Physique.

■ REFERENCES

(1) Horwitz, J. P.; Chua, J.; Noel, M. Nucleosides. V. The Monomesylates of 1-(2′-Deoxy-β-D-lyxofuranosyl)thymine1,2. *J. Org. Chem.* **1964**, *29*, 2076−2078.

(2) Mitsuya, H.; Weinhold, K. J.; Furman, P. A.; St Clair, M. H.; Lehrman, S. N.; Gallo, R. C.; Bolognesi, D.; Barry, D. W.; Broder, S. 3′-Azido-3′-deoxythymidine (BW A509U): an antiviral agent that inhibits the infectivity and cytopathic effect of human T-lymphotropic virus type III/lymphadenopathy-associated virus in vitro. *Proc. Natl. Acad. Sci. U.S.A.* **1985**, *82*, 7096−7100.

(3) Pathak, T. Azidonucleosides: Synthesis, Reactions, and Biological Properties. *Chem. Rev.* **2002**, *102*, 1623−1668.

(4) Müggenburg, F.; Müller, S. Azide-modified Nucleosides as Versatile Tools for Bioorthogonal Labeling and Functionalization. *Chem. Rec.* **2022**, *22*, No. e202100322.

(5) van der Donk, W. A.; Stubbe, J.; Gerfen, G. J.; Bellew, B. F.; Griffin, R. G. EPR Investigations of the Inactivation of E. coli Ribonucleotide Reductase with 2′-Azido-2′-deoxyuridine 5′-Diphosphate: Evidence for the Involvement of the Thiyl Radical of C225-R1. *J. Am. Chem. Soc.* **1995**, *117*, 8908−8916.

(6) Fritscher, J.; Artin, E.; Wnuk, S.; Bar, G.; Robblee, J. H.; Kacprzak, S.; Kaupp, M.; Griffin, R. G.; Bennati, M.; Stubbe, J. Structure of the Nitrogen-Centered Radical Formed during Inactivation of E. coli Ribonucleotide Reductase by 2′-Azido-2′-deoxyuridine-5′-diphosphate: Trapping of the 3′-Ketonucleotide. *J. Am. Chem. Soc.* **2005**, *127*, 7729−7738.

(7) Wen, Z.; Peng, J.; Tuttle, P.; Ren, Y.; Garcia, C.; Debnath, D.; Rishi, S.; Hanson, C.; Ward, S.; Kumar, A.; et al. Electron-mediated Aminyl and Iminyl Radicals from C5-Azido-Modified Pyrimidine Nucleosides Augment Radiation Damage to Cancer Cells. *Org. Lett.* **2018**, *20*, 7400−7404.

(8) Jagetia, G. C.; Aruna, R. Correlation of micronuclei-induction with the cell survival in HeLa cells treated with a base analogue, azidothymidine (AZT) before exposure to different doses of gamma-radiation. *Toxicol. Lett.* **2003**, *139*, 33−43.

(9) Coucke, P. A.; Cottin, E.; Decosterd, L. A. Simultaneous alteration of de novo and salvage pathway to the deoxynucleoside triphosphate pool by (e)-2′-deoxy-(fluoromethylene)cytidine (fmdc) and zidovudine (azt) results in increased radiosensitivity in vitro. *Acta Oncol.* **2007**, *46*, 612−620.

(10) Liao, Z.-K.; Zhou, F.-X.; Luo, Z.-G.; Zhang, W.-J.; Jie, X.; Bao, J.; Han, G.; Zhang, M.-S.; Xie, C.-H.; Zhou, Y-F. Radio-activation of htert promoter in larynx squamous carcinoma cells: An 'indirected-activator' strategy in radio-gene-therapy. *Oncol. Rep.* **2008**, *19*, 281−286.

(11) Zhou, F.-X.; Liao, Z.-K.; Dai, J.; Jie, X.; Xie, C.-H.; Luo, Z.-G.; Liu, S.-Q.; Zhou, Y.-F. Radiosensitization effect of zidovudine on human malignant glioma cells. *Biochem. Biophys. Res. Commun.* **2007**, *354*, 351−356.

(12) Westphal, E. M.; Blackstock, W.; Feng, W.; Israel, B.; Kenney, S. C. Activation of lytic Epstein-Barr virus (EBV) infection by radiation and sodium butyrate in vitro and in vivo: a potential method for treating EBV-positive malignancies. *Cancer Res.* **2000**, *60*, 5781−5788.

(13) Becker, D.; Adhikary, A.; Sevilla, M. D. *Recent Trends in Radiation Chemistry*; Rao, B. S. M.; Wishart, J., Eds.; World Scientific Publishing Co.: Singapore, 2010; pp 509−542.

(14) Becker, D.; Adhikary, A.; Sevilla, M. D. *Charged Particle and Photon Interactions with Matter − Recent Advances, Applications, and Interfaces*; Hatano, Y.; Katsumura, Y.; Mozumder, A., Eds.; CRC Press, Taylor & Francis Group: Boca Raton, 2010; pp 503−541.

(15) Adhikary, A.; Becker, D.; Sevilla, M. D. Electron Spin Resonance of Radicals in Irradiated DNA. In *Applications of EPR in Radiation Research*; Lund, A.; Shiotani, M., Eds.; Springer-Verlag: Berlin, 2014; pp 299−352.

(16) Ma, J.; Denisov, S. A.; Adhikary, A.; Mostafavi, M. Ultrafast Processes Occurring in Radiolysis of Highly Concentrated Solutions of Nucleosides/Tides. *Int. J. Mol. Sci.* **2019**, *20*, 4963.

(17) Becker, D.; Kumar, A.; Adhikary, A.; Sevilla, M. D. γ- and Ion-Beam DNA Radiation Damage: Theory and Experiment. In *DNA Damage, DNA Repair and Disease*; Dizdaroglu, M.; Llyod, R. S., Eds.; Royal Society of Chemistry: London, U.K., 2020; Vol. 2, pp 426−457.
(18) Bernhard, W. A. *'Radical and Radical Ion Reactivity in Nucleic Acid Chemistry'*; Greenberg, M. M., Ed.; John Wiley & Sons, Inc.: New Jersey, 2009; pp 41−68.
(19) Close, D. M. *Radiation-induced Molecular Phenomena in Nucleic Acids: A Comprehensive Theoretical and Experimental Analysis*; Shukla, M. K.; Leszczynski, J., Eds.; Springer-Verlag: Berlin, 2008; pp 493−529.
(20) Ma, J.; Kumar, A.; Muroya, Y.; Yamashita, S.; Sakurai, T.; Denisov, S. A.; Sevilla, M. D.; Adhikary, A.; Seki, S.; Mostafavi, M. Observation of Dissociative Quasi-Free Electron Attachment to Nucleoside via Excited Anion Radical in Solution. *Nat. Commun.* **2019**, *10*, No. 102.
(21) Boudaïffa, B.; Cloutier, P.; Hunting, D.; Huels, M. A.; Sanche, L. Resonant formation of DNA strand breaks by low-energy (3−20 eV) electrons. *Science* **2000**, *287*, 1658−1660.
(22) Fabrikant, I. I.; Eden, S.; Mason, N. J.; Fedor, J. *Recent Progress in Dissociative Electron Attachment: From Diatomics to Biomolecules*, 1st ed.; Elsevier Inc., 2017; p 66.
(23) Alizadeh, E.; Sanche, L. Precursors of Solvated Electrons in Radiobiological Physics and Chemistry. *Chem. Rev.* **2012**, *112*, 5578−5602.
(24) Kumar, A.; Sevilla, M. D. Low-Energy Electron (LEE)-Induced DNA Damage: Theoretical Approaches to Modeling Experiment. In *Handbook of Computational Chemistry*; Leszczynski, J., Ed.; Springer: Dordrecht, The Netherlands, 2015; pp 1−63.
(25) Kumar, A.; Becker, D.; Adhikary, A.; Sevilla, M. D. Reaction of Electrons with DNA: Radiation Damage to Radiosensitization. *Int. J. Mol. Sci.* **2019**, *20*, 3998.
(26) Ma, J.; Denisov, S.; Adhikary, A.; Mostafavi, M. Comment un électron induit un dommage oxydatif dans l'ADN. *l'Actualité Chim.* **2020**, *450*, 13−18.
(27) Gu, J.; Leszczynski, J.; Schaefer, H. F., III Interactions of electrons with bare and hydrated biomolecules: From nucleic acid bases to DNA segments. *Chem. Rev.* **2012**, *112*, 5603−5640.
(28) Aflatooni, K.; Gallup, G. A.; Burrow, P. D. Electron attachment energies of the DNA bases. *J. Phys. Chem. A* **1998**, *102*, 6205−6207.
(29) von Sonntag, C. *Free-Radical-Induced DNA Damage and Its Repair: A Chemical Perspective*; Springer: Berlin, 2006.
(30) von Sonntag, C. *The Chemical Basis of Radiation Biology*; Taylor and Francis: London, 1987.
(31) Li, X.; Cai, Z.; Sevilla, M. D. DFT Calculations of the Electron Affinities of Nucleic Acid Bases: Dealing with Negative Electron Affinities. *J. Phys. Chem. A* **2002**, *106*, 1596−1603.
(32) Ma, J.; Wang, F.; Denisov, S. A.; Adhikary, A.; Mostafavi, M. Reactivity of Prehydrated Electrons towards Nucleobases and Nucleotides in Aqueous Solution. *Sci. Adv.* **2017**, *3*, No. e1701669.
(33) Kozak, W.; Demkowicz, S.; Daśko, M.; Rachon, J.; Rak, J. Modifications at the C(5) Position of Pyrimidine Nucleosides. *Russ. Chem. Rev.* **2020**, *89*, 281−310.
(34) Chomicz, L.; Petrovici, A.; Archbold, I. J.; Adhikary, A.; Kumar, A.; Sevilla, M. D.; Rak, J. An ESR and DFT study of Hydration of the 2′-Deoxyuridine-5-yl Radical: Possible Hydroxyl Radical Intermediate. *Chem. Commun.* **2014**, *50*, 14605−14608.
(35) Ma, J.; Bahry, T.; Denisov, S.; Adhikary, A.; Mostafavi, M. Quasi-free Electron-mediated Radiation Sensitization by C5-Halopyrimidines. *J. Phys. Chem. A* **2021**, *125*, 7967−7975.
(36) Webb, C. F.; Jones, G. D. D.; Ward, J. F.; Moyer, D. J.; Aguilera, J. A.; Ling, L. L. Mechanisms of Radiosensitization in Bromodeoxyuridine-substituted Cells. *Int. J. Radiat Biol.* **1993**, *64*, 695−705.
(37) Lehnert, S. *Radiosensitizers and Radiochemotherapy in the Treatment of Cancer*; CRC Press, Taylor & Francis Group: Boca Raton, 2015; pp 93−118.
(38) Dabaja, B. S.; McLaughlin, P.; Ha, C. S.; Pro, B.; Meyers, C. A.; Seabrooke, L. F.; Wilder, R. B.; Kyritsis, A. P.; Preti, H. A.; Yung, W. K. A.; et al. Primary central nervous system lymphoma: Phase I evaluation of infusional bromodeoxyuridine with whole brain accelerated fractionation radiation therapy after chemotherapy. *Cancer* **2003**, *98*, 1021−1028.
(39) Prados, M. D.; Seiferheld, W.; Sandler, H. M.; Buckner, J. C.; Phillips, T.; Schultz, C.; Urtasun, R.; Davis, R.; Gutin, P.; Cascino, T. L.; et al. Phase III randomized study of radiotherapy plus procarbazine, lomustine, and vincristine with or without BUdR for treatment of anaplastic astrocytoma: final report of RTOG 9404. *Int. J. Radiat. Oncol. Biol. Phys.* **2004**, *58*, 1147−1152.
(40) Schurmann, R.; Vogel, S.; Ebel, K.; Bald, I. The physico-chemical basis of DNA radiosensitization - implications for cancer radiation therapy. *Chem. − Eur. J.* **2018**, *24*, 1.
(41) Adhikary, A.; Khanduri, D.; Pottiboyina, V.; Rice, C. T.; Sevilla, M. D. Formation of Aminyl Radicals on Electron Attachment to AZT: Abstraction from the Sugar Phosphate Backbone versus One-Electron Oxidation of Guanine. *J. Phys. Chem. B* **2010**, *114*, 9289−9299.
(42) Mudgal, M.; Dang, T.; Sobczak, A.; Lumpuy, D.; Dutta, P.; Ward, S.; Ward, K.; Alahmadi, M.; Kumar, A.; Sevilla, M. D.; et al. Site of Azido Substitution in the Sugar Moiety of Azidopyrimidine Nucleosides Influences the Reactivity of Aminyl Radicals Formed by Dissociative Electron Attachment. *J. Phys. Chem. B* **2020**, *124*, 11357−11370.
(43) Mudgal, M.; Rishi, S.; Lumpuy, D. A.; Curran, K. A.; Verley, K. L.; Sobczak, A. J.; Dang, T. P.; Sulimoff, N.; Kumar, A.; Sevilla, M. D.; et al. Prehydrated One-Electron Attachment to Azido-Modified Pentofuranoses: Aminyl Radical Formation, Rapid H-Atom Transfer, and Subsequent Ring Opening. *J. Phys. Chem. B* **2017**, *121*, 4968−4980.
(44) Tanaka, H.; Hayakawa, H.; Iijima, S.; Haraguchi, K.; Miyasaka, T. Lithiation of 3′,5′-O-(tetraisopropyldisiloxane-1,3-diyl)-2′-deoxyuridine: synthesis of 6-substituted 2′-deoxyuridines. *Tetrahedron* **1985**, *41*, 861−866.
(45) Wojnárovits, L.; Takács, E. Rate constants of sulfate radical anion reactions with organic molecules: A review. *Chemosphere* **2019**, *220*, 1014−1032.
(46) Tomasi, J.; Mennucci, B.; Cammi, R. Quantum Mechanical Continuum Solvation Models. *Chem. Rev.* **2005**, *105*, 2999−3094.
(47) Frisch, M. J.; Trucks, G. W.; Schlegel, H. B.; Scuseria, G. E.; Robb, M. A.; Cheeseman, J. R.; Scalmani, G.; Barone, V.; Petersson, G. A.; Nakatsuji, H.et al. *Gaussian 16*, Revision A.03; Gaussian, Inc.: Wallingford, CT, 2016.
(48) Jmol: an open-source browser-based HTML5 viewer and stand-alone Java viewer for chemical structures in 3D. http://jmol.sourceforge.net/ (accessed October 02, 2021).
(49) Allouche, A.-R. Gabedit—A Graphical User Interface for Computational Chemistry Softwares. *J. Comput. Chem.* **2011**, *32*, 174−182.
(50) Kumar, A.; Sevilla, M. D. Excited States of One-Electron Oxidized Guanine-Cytosine Base Pair Radicals: A Time Dependent Density Functional Theory Study. *J. Phys. Chem. A* **2019**, *123*, 3098−3108.

https://doi.org/10.1021/acs.jpcb.2c08257
J. Phys. Chem. B 2023, 127, 1563−1571